Observation of $\chi_{c0} \to \Sigma^+\bar{\Sigma}^-\eta$ and evidence for $\chi_{c1,2} \to \Sigma^+\bar{\Sigma}^-\eta$

M. Ablikim *et al.*[*]
(BESIII Collaboration)

(Received 18 October 2024; accepted 25 November 2024; published 16 December 2024)

Using $(27.12 \pm 0.14) \times 10^8$ $\psi(3686)$ events collected with the BESIII detector, the decay $\chi_{c0} \to \Sigma^+\bar{\Sigma}^-\eta$ is observed for the first time with a signal significance of 7.0σ, and evidence for $\chi_{c1} \to \Sigma^+\bar{\Sigma}^-\eta$ and $\chi_{c2} \to \Sigma^+\bar{\Sigma}^-\eta$ is found with signal significances of 4.3σ and 4.6σ, respectively. The branching fractions are determined to be $\mathcal{B}(\chi_{c0} \to \Sigma^+\bar{\Sigma}^-\eta) = (1.26 \pm 0.20 \pm 0.13) \times 10^{-4}$, $\mathcal{B}(\chi_{c1} \to \Sigma^+\bar{\Sigma}^-\eta) = (5.10 \pm 1.21 \pm 0.67) \times 10^{-5}$, and $\mathcal{B}(\chi_{c2} \to \Sigma^+\bar{\Sigma}^-\eta) = (5.46 \pm 1.18 \pm 0.50) \times 10^{-5}$, where the first uncertainties are statistical, and the second ones are systematic.

DOI: 10.1103/PhysRevD.110.112013

I. INTRODUCTION

In the investigations of $e^+e^- \to \Lambda\bar{\Lambda}\eta$, $e^+e^- \to \Lambda\bar{\Lambda}\phi$, $J/\psi \to \gamma p\bar{p}$ and $\psi(3686) \to \gamma p\bar{p}$, unexpected enhancements have been detected near the mass thresholds of $\Lambda\bar{\Lambda}$ and $p\bar{p}$ pairs [1–3]. Several theoretical models have been suggested to explain these enhancements, including the one-boson-exchange potential model, $^3P_0$ meson decay model, quark potential model and quark-pair creation model [4,5]. Due to a larger phase space available for χ_{cJ} decays compared to J/ψ decays, a greater range of possible final states may be explored in χ_{cJ} decays for baryon-antibaryon pair mass threshold enhancements.

The exploration of charmonium decays is crucial to improve our understanding of quantum chromodynamics (QCD) [6]. So far, only a few investigations have been conducted on the decays $\chi_{cJ} \to B\bar{B}M$ (where B represents a baryon and M denotes a meson), such as $\chi_{cJ} \to \Lambda\bar{\Lambda}\eta$ [7]. Therefore, further studies are highly desirable to explore the properties of χ_{cJ} particles.

In this paper, we report the first observation of $\chi_{c0} \to \Sigma^+\bar{\Sigma}^-\eta$, evidence for $\chi_{c1,2} \to \Sigma^+\bar{\Sigma}^-\eta$, and searches for enhancements near the $\Sigma^+\bar{\Sigma}^-$ mass threshold and possible excited states of Σ^+, where the $\chi_{c0,1,2}$ are produced in $\psi(3683)$ radiative decays. The analysis uses $(27.12 \pm 0.14) \times 10^8$ $\psi(3686)$ events [8] collected with the BESIII detector in 2009, 2012 and 2021.

II. BESIII DETECTOR AND MONTE CARLO SIMULATION

The BESIII detector [9] records symmetric e^+e^- collisions provided by the BEPCII storage ring [10] in the center-of-mass energy range from 2.0 to 4.95 GeV, with a peak luminosity of 1×10^{33} cm^{-2} s^{-1} achieved at $\sqrt{s} = 3.77$ GeV. BESIII has collected large data samples in this energy region [11–13]. The cylindrical core of the BESIII detector covers 93% of the full solid angle and consists of a helium-based multilayer drift chamber (MDC), a plastic scintillator time-of-flight system (TOF), and a CsI (Tl) electromagnetic calorimeter (EMC), which are all enclosed in a superconducting solenoidal magnet providing a 1.0 T magnetic field. The solenoid is supported by an octagonal flux-return yoke with resistive plate counter muon identification modules interleaved with steel. The charged-particle momentum resolution at 1 GeV/c is 0.5%, and the specific energy loss (dE/dx) resolution is 6% for electrons from Bhabha scattering. The EMC measures photon energies with a resolution of 2.5% (5%) at 1 GeV in the barrel (end cap) region. The time resolution in the TOF barrel region is 68 ps, while that in the end cap region was 110 ps. The end cap TOF system was upgraded in 2015 using multigap resistive plate chamber technology, providing a time resolution of 60 ps, which benefits 86% of the data used in this analysis [14].

Monte Carlo (MC) simulated data samples produced with a Geant4-based [15] software package, which includes the geometric description of the BESIII detector and the detector response, are used to determine detection efficiencies and to estimate backgrounds. The simulation models the beam energy spread and initial state radiation (ISR) in the e^+e^- annihilations with the generator KKMC [16]. The inclusive MC sample includes the production of the $\psi(3686)$ resonance, the ISR production of the J/ψ, and the continuum processes incorporated in KKMC, with

[*]Full author list given at the end of the article.

approximately 2.8 billion events. All particle decays are modeled with EvtGen [17] using branching fractions either taken from the Particle Data Group (PDG) [18], when available, or otherwise estimated with LUNDCHARM [19]. In this analysis, we use the phase space (PHSP) signal MC events (3 million events for each channel) to determine the efficiency. The BODY3 [20] signal MC events are also generated to estimate systematic uncertainties of PHSP MC, by reweighting the PHSP MC Dalitz distribution to match the background-subtracted data.

III. EVENT SELECTION

The $\Sigma^+(\bar{\Sigma}^-)$ candidate is reconstructed via $\Sigma^+(\bar{\Sigma}^-) \to p\pi^0(\bar{p}\pi^0)$, and the η candidate is reconstructed via $\eta \to \gamma\gamma$.

Photon candidates are identified using isolated showers in the EMC. The deposited energy of each shower must be more than 25 MeV in the barrel region ($|\cos\theta| < 0.80$), where θ is the polar angle with respect to the z axis, which is the symmetry axis of the MDC, and more than 50 MeV in the end cap region ($0.86 < |\cos\theta| < 0.92$). To exclude showers that originate from charged tracks, the angle subtended by the EMC shower and the position of the closest charged track at the EMC must be greater than 10 degrees as measured from the interaction point (IP). To suppress electronic noise and showers unrelated to the event, the difference between the EMC shower time and the event start time is required to be within [0, 700] ns. The number of photon candidates is required to be at least seven.

Candidate events must contain at least one positively charged track and one negatively charged track. The polar angle of each track measured in the MDC is required to satisfy $|\cos\theta| < 0.93$. The dE/dx information in the MDC is combined with the time of flight from the TOF detector to identify the type of particle (PID). For this purpose, confidence levels for pion, proton and kaon hypotheses are calculated, and tracks are assigned to the hypothesis with the highest confidence level. The $\Sigma^+(\bar{\Sigma}^-)$ candidate is reconstructed by combining pairs of $p(\bar{p})$ and π^0 candidates. Because of the relatively large decay length of the $\Sigma^+(\bar{\Sigma}^-)$ particle, the $p(\bar{p})$ candidate is required to have a distance of closest approach to the IP less than 15 cm along the z-axis, and less than 2 cm in the transverse plane.

Next we select π^0 candidates from $\gamma\gamma$ pairs with invariant masses within $[0.08, 0.20]$ GeV/c^2, which roughly corresponds to the 3σ region around the fitted central value. A π^0 candidate must satisfy a one constraint (1C) kinematic fit with the $\gamma\gamma$ mass constrained to the π^0 mass. At least two π^0 candidates are required. Of the remaining photons, the one resulting in the largest value of ΔM as defined in Eq. (1) is assigned as the radiative photon (γ_E), and the others are assigned as possibly decaying from the η.

In order to suppress background and improve the resolution, six-constraint (6C) kinematic fits (with constraints on total four momentum of the final state particles and the masses of the two π^0 candidates) are applied to all the potential final state combinations, and the combination with the smallest $\chi^2_{\rm 6C}$ is kept. Further, to match $p(\bar{p})$ with its π^0 to identify $\Sigma^+(\bar{\Sigma}^-)$, only the combination with the smallest value of

$$\Delta M = ((M_{p\pi^0} - m_{\Sigma^+})^2 + (M_{\bar{p}\pi^0} - m_{\bar{\Sigma}^-})^2 + (M_{\gamma\gamma} - m_\eta)^2)^{\frac{1}{2}} \quad (1)$$

is retained, where $M_{p\pi^0}(M_{\bar{p}\pi^0})$ is the invariant mass of the $p\pi^0(\bar{p}\pi^0)$ system, $M_{\gamma\gamma}$ is the invariant mass of the $\gamma\gamma$ system, $m_{\Sigma^+}(m_{\bar{\Sigma}^-})$ is the known mass of $\Sigma^+(\bar{\Sigma}^-)$ [18], and m_η is the known mass of η [18]. A figure of merit (FOM) optimization is performed for the $\chi^2_{\rm 6C}$ requirement, based on maximizing the value of $\frac{S}{\sqrt{S+B}}$ (where S is the signal yield from the signal MC sample and B is the background yield from the inclusive MC sample normalized to the integrated luminosity of data). The optimized selection criterion is $\chi^2_{\rm 6C} < 45$.

Various background channels are suppressed by requiring $\chi^2_{\rm signal} < \chi^2_{\rm bkg}$, where $\chi^2_{\rm signal}$ is the 4C χ^2 under the hypothesis of $\chi_{cJ} \to \Sigma^+\bar{\Sigma}^-\eta$, while $\chi^2_{\rm bkg}$ is the 4C χ^2 of background channels by adding or subtracting one photon, satisfying the good photon requirements.

In the following, particle momenta updated by the 6C fit are used. To reject $\chi_{cJ} \to \gamma J/\psi(\to \Sigma^+\bar{\Sigma}^-\gamma)$, we require $|M(\Sigma^+\bar{\Sigma}^-\gamma_E) - 3.091\ \text{GeV}/c^2| > 0.056\ \text{GeV}/c^2$, where γ_E is the photon from the $\psi(3686)$. To reject $\chi_{cJ} \to \Sigma^+\bar{\Sigma}^-\pi^0$, we require $|M(\gamma_E\gamma_1) - 0.132\ \text{GeV}/c^2| > 0.018\ \text{GeV}/c^2$ and $|M(\gamma_E\gamma_2) - 0.137\ \text{GeV}/c^2| > 0.044\ \text{GeV}/c^2$, where γ_1 and γ_2 are the photons from the η, which are the other two good photons in addition to the previously mentioned γ_E and π^0 candidates. The photon with higher energy is designated as γ_1, while the other is denoted as γ_2. The mass windows for these vetoes are centered around the fitted value from data, which slightly differ from the PDG values. The widths of the mass windows are also obtained from the fit to data and correspond to the 3σ region around the fitted central value. Other potential backgrounds, including $\chi_{cJ} \to \eta\Delta^+\bar{\Delta}^-$, $\chi_{cJ} \to \eta' p\bar{p}$, and $\chi_{cJ} \to \pi^0\Sigma^+\bar{\Sigma}^-$, are investigated by analyzing the $\psi(3686)$ inclusive MC sample with TopoAna [21]. After the above requirements, only a small fraction (less than 1% of the signal yield) of background events survive the selection criteria and can be safely ignored. We impose the same event selection criteria on the continuum data taken at $\sqrt{s} = 3.650$ GeV, and only one event survives. After scaling to the $\psi(3686)$ data sample using $f_{\rm scale} = \frac{\mathcal{L}_{\psi(3686)}}{\mathcal{L}_{3.65}} \times \frac{3.65^2}{3.686^2}$, where the $\mathcal{L}_{\psi(3686)}$ and $\mathcal{L}_{3.65}$ are the luminosities of the $\psi(3686)$ data and continuum data samples, respectively, the continuum contribution is also found to be negligible. The luminosity of the continuum data sample is 445.5 pb^{-1}, while the luminosity of $\psi(3686)$ data sample is 3877 pb^{-1}.

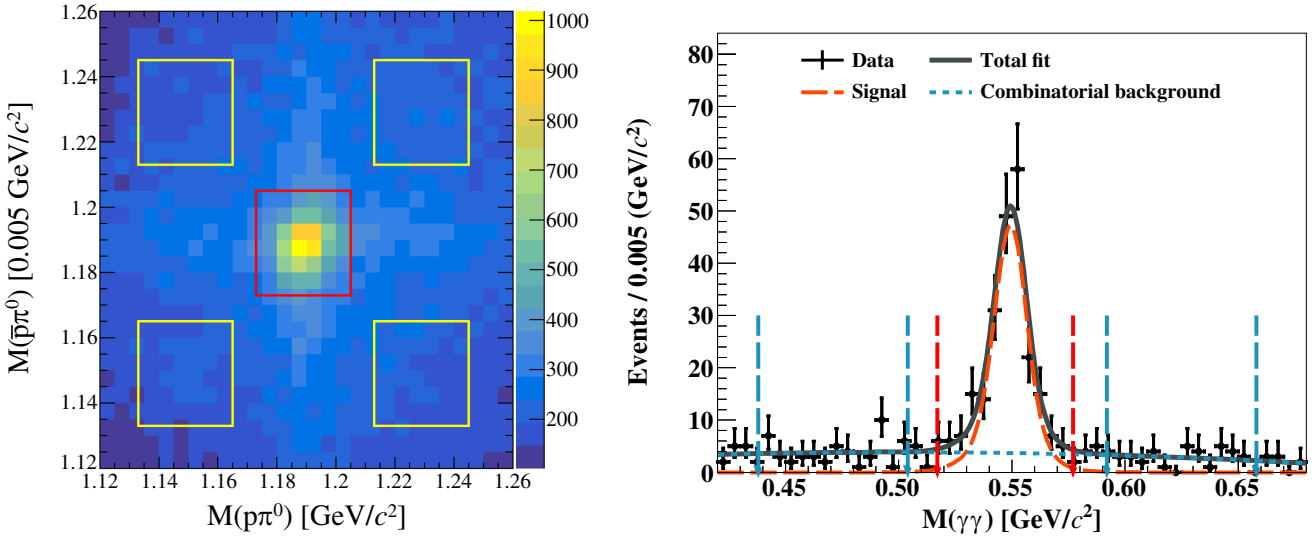

FIG. 1. Distributions of (left) $M(\bar{p}\pi^0)$ versus $M(p\pi^0)$ and (right) $M(\gamma\gamma)$ of the accepted candidates. In the left figure, the red box represents the $\Sigma^+\bar{\Sigma}^-$ signal region, and the yellow boxes are the $\Sigma^+\bar{\Sigma}^-$ sideband region. In the right figure, the red dashed line represents the fitted η signal, and the blue dashed line is the combinatorial background. The gray line is the total fit. The red arrows denote the η signal region, while the blue arrows denote the η sideband region.

The distributions of $M(\bar{p}\pi^0)$ versus $M(p\pi^0)$ and $M(\gamma\gamma)$ with all the selection criteria are shown in Fig. 1. The $\Sigma^+/\bar{\Sigma}^-$ signal mass window of $M(p\pi)$ is chosen as $[1.174, 1.204]$ GeV/c^2, and the sideband regions are defined by $[1.139, 1.169]$ GeV/c^2 and $[1.209, 1.239]$ GeV/c^2. The four squares with equal areas around the signal region are taken as the two dimensional (2D) $\Sigma^+\bar{\Sigma}^-$ sideband regions. The η signal mass window is taken as $M(\gamma\gamma) \in [0.517, 0.577]$ GeV/c^2, and the η sideband regions are $[0.448, 0.508]$ GeV/c^2 and $[0.588, 0.648]$ GeV/c^2.

IV. SIGNAL YIELD DETERMINATION

The signal yields of χ_{cJ} decays are determined by performing a simultaneous fit to the $M(\Sigma^+\bar{\Sigma}^-\gamma\gamma)$ distributions for events in both the η signal and sideband regions, as shown in Fig. 2.

For the fit to the events in the η signal region, shown in Fig. 2 (right), the probability density functions of the χ_{cJ} signals are modeled by individual simulated MC shapes convolved with a Gaussian resolution function that accounts for the resolution difference between data and MC simulation. The combinatorial background is described by a second order Chebyshev polynomial function. The non-η background is constrained by the simultaneous fit to the events in the η sideband region. The non-$\Sigma^+\bar{\Sigma}^-$ background is fixed to the number obtained from the non-$\Sigma^+\bar{\Sigma}^-$ background estimated by the $\Sigma^+\bar{\Sigma}^-$ sideband region of data as shown in Fig. 1 (right) with a scale factor of 0.25, since the $\Sigma^+\bar{\Sigma}^-$ sideband region is four times larger than the $\Sigma^+\bar{\Sigma}^-$ signal region.

For the fit to the η sideband region, simulated MC shape of $\chi_{cJ} \to \Sigma^+\bar{\Sigma}^-\gamma\gamma$ convolved with a Gaussian resolution function is used for the χ_{cJ} signal shapes. The combinatorial background is described by a second order Chebyshev polynomial function. The non-$\Sigma^+\bar{\Sigma}^-$ background is again constrained by the number of events in the $\Sigma^+\bar{\Sigma}^-$ sideband region with a scale factor of 0.25. To determine the scale factor between the η signal and sideband regions, f_η, a fit is performed on the $M(\gamma\gamma)$ spectrum, as shown in Fig. 1 (right), in which the simulated signal MC shape convolved with a Gaussian function is used to model the η signal and a polynomial function is used to describe the combinatorial background. The scale factor f_η is determined to be 0.547 ± 0.067.

For the above two fits, the fraction of non-$\Sigma^+\bar{\Sigma}^-$ background events in the $\Sigma^+\bar{\Sigma}^-$ sideband region [denoted as the four yellow boxes in Fig. 1(left)] are 11.4% in the η signal region and 37.9% in the η sideband region. The signal yields for $\chi_{c0,1,2} \to \Sigma^+\bar{\Sigma}^-\eta$ are 74 ± 12, 36 ± 8 and 35 ± 8, with signal significances of 7.0σ, 4.3σ, and 4.6σ, respectively. The signal significance is determined by examining the difference in log-likelihood as each signal is individually excluded in the fit, taking the changes in the degrees of freedom into account. The systematic uncertainties are already considered in the evaluation of the signal significance.

The branching fractions of $\chi_{cJ} \to \Sigma^+\bar{\Sigma}^-\eta$ are calculated by

$$\mathcal{B}(\chi_{cJ} \to \Sigma^+\bar{\Sigma}^-\eta) = \frac{N_{\rm fit}}{N_{\psi(3686)} \cdot \mathcal{B}(\psi(3686) \to \gamma\chi_{cJ}) \cdot \prod_i \mathcal{B}_i \cdot \epsilon}, \quad (2)$$

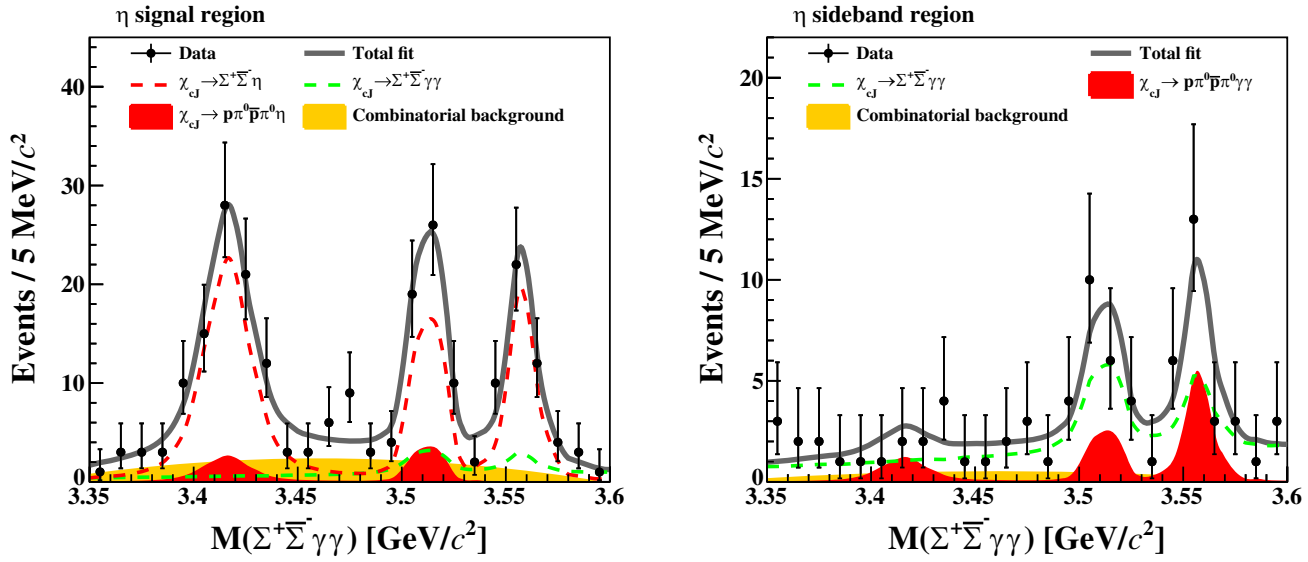

FIG. 2. Simultaneous fit to the $M(\Sigma^+\bar{\Sigma}^-\gamma\gamma)$ distributions in the η signal (left) and sideband (right) regions. In the left figure, the red dashed line is the signal, the red histogram is the fixed contribution from the non-$\Sigma^+\bar{\Sigma}^-$ sideband region of data in the η signal region, and the green dashed line is the background contribution constrained by the fit to the η sideband. Additionally, the orange histogram is the combinatorial background. The gray line is the total fit. In the right figure, the green line is from the simulated $\chi_{cJ}\to\Sigma^+\bar{\Sigma}^-\gamma\gamma$ shape, and the red histogram is the fixed contribution from the non-$\Sigma^+\bar{\Sigma}^-$ background estimated by the $\Sigma^+\bar{\Sigma}^-$ sideband region of data.

where $N_{\rm fit}$ is the fitted signal yield of χ_{cJ}, $N_{\psi(3686)}$ is the number of $\psi(3686)$ events, $\mathcal{B}(\psi(3686)\to\gamma\chi_{cJ})$ is the branching fractions of $\psi(3696)\to\gamma\chi_{cJ}$, $\prod_i\mathcal{B}_i$ is the product of branching fractions of the intermediate decays, including $\mathcal{B}(\Sigma^+\to p\pi^0)=(51.57\pm0.30)\%$, $\mathcal{B}(\bar{\Sigma}^-\to\bar{p}\pi^0)=(51.57\pm0.30)\%$, $\mathcal{B}(\pi^0\to\gamma\gamma)=(98.823\pm0.034)\%$ and $\mathcal{B}(\eta\to\gamma\gamma)=(39.36\pm0.18)\%$, which are taken from the PDG [18], and ϵ is the detection efficiency. The results of branching fractions are listed in Table I.

The background subtracted $M(\Sigma^+\bar{\Sigma}^-)$, $M(\Sigma^+\eta)$, and $M(\bar{\Sigma}^-\eta)$ distributions of data are examined for possible intermediate structures, and no obvious structure is observed with the current statistics. The background-subtracted data distributions are derived by subtracting the corresponding histograms of the sideband regions, which is adjusted by their scaling factors, from the total histogram

$$h_{\rm background-subtracted}=h_{\rm total}-f_\eta\times h_{\eta\rm SD}-f_{2D}\times h_{2D\rm SD}. \quad (3)$$

TABLE I. Fitted signal yield ($N_{\rm fit}$), detection efficiency (ϵ), statistical significance, and branching fraction ($\mathcal{B}$). The first and second uncertainties are statistical and systematic, respectively.

Decay	$N_{\rm fit}$	Significance	$\epsilon(\%)$	$\mathcal{B}(10^{-5})$
$\chi_{c0}\to\Sigma^+\bar{\Sigma}^-\eta$	74 ± 12	7.0σ	2.18	$12.6\pm2.0\pm1.3$
$\chi_{c1}\to\Sigma^+\bar{\Sigma}^-\eta$	36 ± 8	4.3σ	2.61	$5.10\pm1.21\pm0.67$
$\chi_{c2}\to\Sigma^+\bar{\Sigma}^-\eta$	35 ± 8	4.6σ	2.46	$5.46\pm1.18\pm0.50$

The values of $M(\Sigma^+\bar{\Sigma}^-)$, $M(\Sigma^+\eta)$ and $M(\bar{\Sigma}^-\eta)$ are taken from the 6C fit. The data-MC comparison is shown in Fig. 3.

V. SYSTEMATIC UNCERTAINTIES

The systematic uncertainties considered are from the tracking and PID efficiencies, photon reconstruction, kinematic fit, mass windows, mass vetoes, signal and background shape, fit range, scale factor f_η, non-$\Sigma^+\bar{\Sigma}^-$ sideband background level, possible intermediate states, external branching fractions, number of $\psi(3686)$ events, and MC statistics. Each of these uncertainties is discussed in detail below.

(i) *Tracking*: The systematic uncertainties due to the tracking are estimated to be 0.7% for p and 1.0% for $\bar{p}$ [22]. Adding them linearly gives the total systematic uncertainty due to p and $\bar{p}$ tracking to be 1.7%.

(ii) *$p\bar{p}$ PID*: The systematic uncertainty due to the PID efficiency is estimated to be 0.5% and 0.6% for the proton and antiproton [23], respectively. Adding them linearly gives a total systematic uncertainty due to p and $\bar{p}$ PID of 1.1%.

(iii) *Photon reconstruction*: The photon-detection efficiency is studied using a control sample of $e^+e^-\to\gamma\mu^+\mu^-$ events. The difference in the photon detection efficiencies between data and MC simulation, 0.5%, is assigned as the systematic uncertainty for each photon.

(iv) *Kinematic fit*: The systematic uncertainty associated with the 6C kinematic fit is assigned as the difference between the efficiencies before and after the

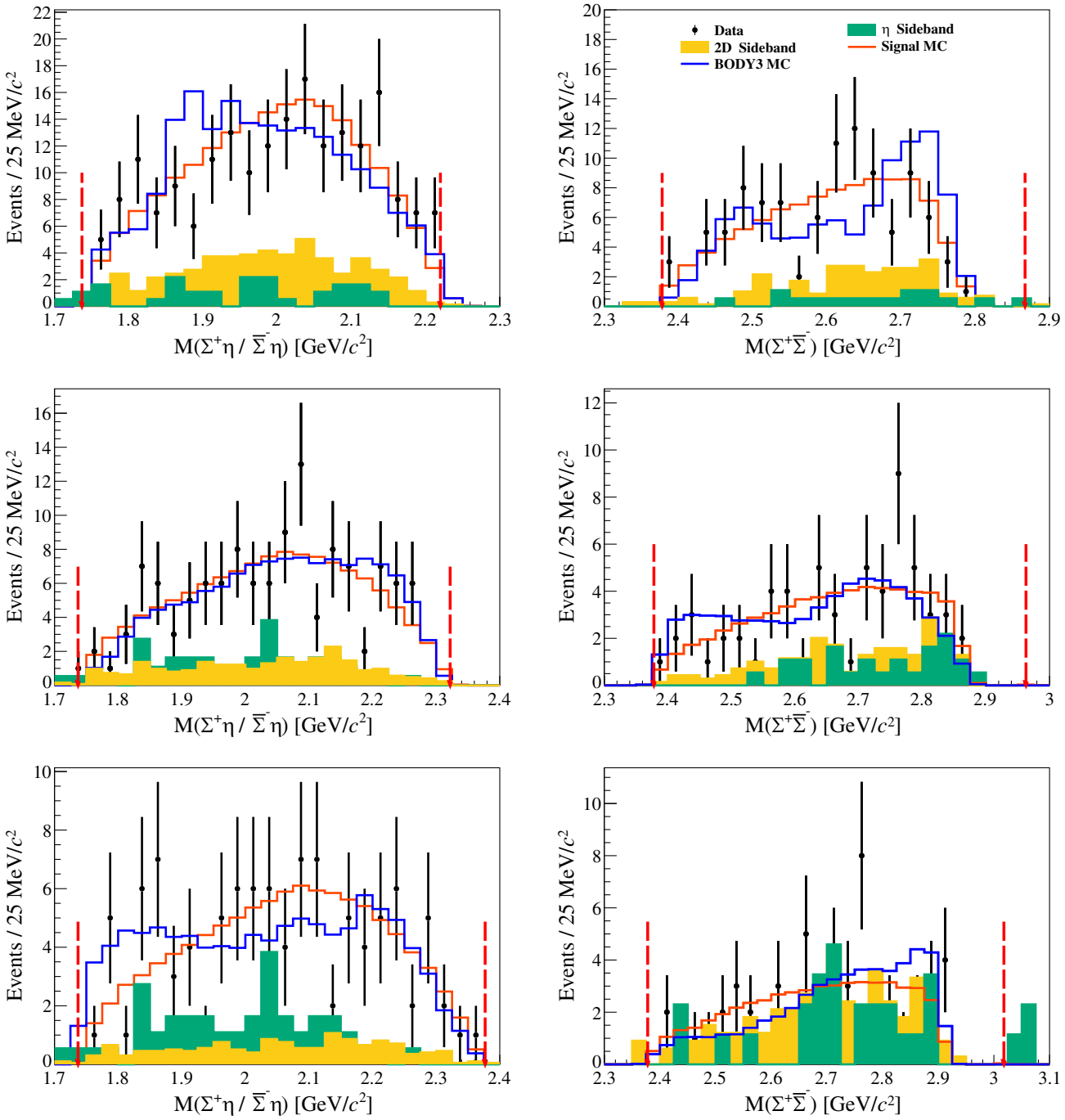

FIG. 3. Comparisons of $M(\bar{\Sigma}^-\eta/\Sigma^+\eta)$ (left) and $M(\Sigma^+\bar{\Sigma}^-)$ (right) of (top) χ_{c0}, (middle) χ_{c1}, (bottom) χ_{c2}. The black dots with error bars represent the data. The green filled histogram indicates the 2D background, while the yellow filled histogram represents events in the η sideband. The red line corresponds to the PHSP Monte Carlo simulation, and the blue line represents the BODY3 Monte Carlo simulation. The kinematic limits are marked by the red dashed arrows.

helix correction [24], which are 0.8%, 0.4% and 0.4% for $\chi_{c0,1,2} \to \Sigma^+\bar{\Sigma}^-\eta$, respectively.

(v) *Mass windows*: To estimate the systematic uncertainties due to the mass windows of Σ^+, $\bar{\Sigma}^-$ and η, we use the control sample of $\psi(3686) \to \Sigma^+\bar{\Sigma}^-$ and $\psi(3686) \to \eta\phi$. By comparing the difference between data and MC simulation, the systematic uncertainty due to the Σ^+ mass window is found to be negligible for $\chi_{c0,1,2}$; the systematic uncertainty due to the $\bar{\Sigma}^-$ mass window is assigned to be 0.3% for $\chi_{c0,1,2}$; and the systematic uncertainty due to the η mass window is assigned to be 1.1% for $\chi_{c0,1,2}$.

(vi) *Mass vetoes*: To estimate the systematic uncertainties of the mass vetoes, we examine the branching

fractions after enlarging or shrinking the veto region. For different background vetoes, we vary the corresponding mass windows for seven times with a step of 1 or 2 MeV/c^2. For each case, the deviation between the alternative and nominal fits is defined as $\zeta = \frac{|\mathcal{B}_{\rm nominal}-\mathcal{B}_{\rm test}|}{\sqrt{|\sigma^2_{\mathcal{B},\rm nominal}-\sigma^2_{\mathcal{B},\rm test}|}}$, where $\mathcal{B}$ is the branching fractions of $\chi_{cJ} \to \Sigma^+\bar{\Sigma}^-\eta$ and σ is its statistical uncertainty. If ζ is less than 2.0, the associated systematic uncertainty is negligible according to the Barlow test [25]. The largest relative difference is assigned as the systematic uncertainty.

(vii) *Fit range*: The systematic uncertainties due to the fit range are examined by enlarging and shrinking the fit range seven times with a step of 4 MeV/c^2, and the Barlow test is performed with the same method mentioned above, and the systematic uncertainties are negligible for $\chi_{c0,1,2}$.

(viii) *Signal shape*: The systematic uncertainty arising from the signal shape is evaluated by varying the parameters of the resolution Gaussian within their statistical uncertainties, and the larger difference is taken as the systematic uncertainties, which are 0.8%, 1.8% and 1.5% for $\chi_{c0,1,2} \to \Sigma^+\bar{\Sigma}^-\eta$, respectively.

(ix) *Background shape*: The systematic uncertainty due to the background shape is estimated by replacing the second order Chebyshev polynomial function with a first or third order Chebyshev polynomial function. The largest differences in the measured branching fractions are taken as the systematic uncertainties, which are 6.3%, 8.6% and 2.9% for $\chi_{c0,1,2} \to \Sigma^+\bar{\Sigma}^-\eta$, respectively.

(x) *Scale factor* f_η: The scale factor f_η directly affects the fitted signal yields. The associated systematic uncertainty is estimated by changing the η sideband region by $\pm 1\sigma$, where σ is the mass resolution of η. The largest differences of the branching fractions, which is negligible for $\chi_{c0} \to \Sigma^+\bar{\Sigma}^-\eta$, and are 3.5% and 3.4% for $\chi_{c1,2} \to \Sigma^+\bar{\Sigma}^-\eta$, respectively, are taken as the systematic uncertainties.

(xi) *Non-*$\Sigma^+\bar{\Sigma}^-$ *background level*: The systematic uncertainties induced by the non-$\Sigma^+\bar{\Sigma}^-$ background subtraction are estimated by changing the number of background events in the $\Sigma^+\bar{\Sigma}^-$ sideband region by $\pm 1\sigma$, where σ is the statistical uncertainty of background events. The differences between the nominal and adjusted values are assigned as the systematic uncertainties, which are 4.8%, 6.3% and 3.3% for $\chi_{c0,1,2} \to \Sigma^+\bar{\Sigma}^-\eta$, respectively.

(xii) *Possible intermediate states*: Considering the difference between data and PHSP signal MC sample, we develop a data-driven BODY3 model [20]. The Dalitz plot of $M^2_{\Sigma^+\eta}$ versus $M^2_{\bar{\Sigma}^-\eta}$ obtained from data is taken as input for the BODY3 model, which is corrected for backgrounds and efficiencies. To estimate the systematic uncertainty associated with the possible intermediate structures, we compare the efficiencies based on the PHSP and BODY3 signal MC samples. The differences are assigned as the systematic uncertainties, which are 2.1%, 3.6% and 3.9% for $\chi_{c0,1,2} \to \Sigma^+\bar{\Sigma}^-\eta$, respectively.

(xiii) *External branching fractions*: The branching fractions of $\psi(3686) \to \gamma\chi_{cJ}, \Sigma^+ \to p\pi^0, \bar{\Sigma}^- \to \bar{p}\pi^0$, $\eta \to \gamma\gamma$, and $\pi^0 \to \gamma\gamma$ are taken from the PDG [18]. Their uncertainties are 2.4%, 2.8% and 2.4% for $\chi_{c0,1,2} \to \Sigma^+\bar{\Sigma}^-\eta$, respectively.

(xiv) *Number of* $\psi(3686)$ *events*: The number of $\psi(3686)$ events is determined with the inclusive hadronic $\psi(3686)$ decays, and its uncertainty is assigned as 0.5% [8].

(xv) *MC statistics*: Using simulated signal events of all the decay modes, the statistical uncertainty in the efficiency is $\Delta_\epsilon = \sqrt{\epsilon(1-\epsilon)/N}$, where ϵ is the reconstruction efficiency after all the event selection, and N is the number of generated events. The uncertainties for the MC statistics, estimated as Δ_ϵ/ϵ are 0.4%, 0.4% and 0.4% for $\chi_{c0,1,2}$, respectively.

The systematic sources and their contributions are summarized in Table II. The total systematic uncertainty for each signal decay is obtained by adding all of them in quadrature.

TABLE II. The relative systematic uncertainties (in unit of %) in the measurements of the branching fractions.

Source	χ_{c0}	χ_{c1}	χ_{c2}
Tracking	1.7	1.7	1.7
$p(\bar{p})$ PID	1.1	1.1	1.1
Photon reconstruction	3.5	3.5	3.5
Kinematic fit	0.8	0.4	0.4
Σ^+ mass window	...	...	...
$\bar{\Sigma}^-$ mass window	0.2	0.2	0.2
η mass window	1.1	1.1	1.1
Veto $\pi^0(\gamma_1\gamma_E)$	...	...	...
Veto $\pi^0(\gamma_2\gamma_E)$	...	...	...
Veto J/ψ	3.3	...	...
Fit range	...	...	...
Signal shape	...	1.4	0.4
Background shape	6.3	8.6	2.9
Scale factor f_η	...	3.5	4.4
Non-$\Sigma^+\bar{\Sigma}^-$ background level	4.8	6.3	3.3
Possible intermediate states	2.1	3.6	3.9
External branching fractions	2.4	2.8	2.4
Total number of $\psi(3686)$ events	1.0	1.0	1.0
MC statistics	0.4	0.4	0.4
Total	10.4	13.2	9.2

VI. SUMMARY

By using $(27.12 \pm 0.14) \times 10^8$ $\psi(3686)$ events taken by the BESIII detector, the decay $\chi_{c0} \to \Sigma^+\bar{\Sigma}^-\eta$ is observed for the first time with a statistical significance of 7.0σ. Evidence for $\chi_{c1} \to \Sigma^+\bar{\Sigma}^-\eta$ and $\chi_{c2} \to \Sigma^+\bar{\Sigma}^-\eta$ is found with statistical significance of 4.3σ and 4.6σ, respectively. The branching fractions of these decays are determined to be $\mathcal{B}(\chi_{c0} \to \Sigma^+\bar{\Sigma}^-\eta) = (1.26 \pm 0.20 \pm 0.13) \times 10^{-4}$, $\mathcal{B}(\chi_{c1} \to \Sigma^+\bar{\Sigma}^-\eta) = (5.10 \pm 1.21 \pm 0.67) \times 10^{-5}$ and $\mathcal{B}(\chi_{c2} \to \Sigma^+\bar{\Sigma}^-\eta) = (5.46 \pm 1.18 \pm 0.50) \times 10^{-5}$, where the first and second uncertainties are statistical and systematic, respectively. With current statistical precision, no obvious intermediate structure is observed in these decays. In order to further understand the characteristics of χ_{cJ} mesons, theoretical investigations of these decay channels are of great importance.

ACKNOWLEDGMENTS

The BESIII Collaboration thanks the staff of BEPCII and the IHEP computing center for their strong support. This work is supported in part by National Key R&D Program of China under Contracts No. 2020YFA0406300, No. 2020YFA0406400; National Natural Science Foundation of China (NSFC) under Contracts No. 11635010, No. 11735014, No. 11835012, No. 11935015, No. 11935016, No. 11935018, No. 11961141012, No. 12025502, No. 12035009, No. 12035013, No. 12061131003, No. 12192260, No. 12192261, No. 12192262, No. 12192263, No. 12192264, No. 12192265, No. 12221005, No. 12225509, No. 12235017, No. 12150004; Program of Science and Technology Development Plan of Jilin Province of China under Contract No. 20210508047RQ and No. 20230101021JC; the Chinese Academy of Sciences (CAS) Large-Scale Scientific Facility Program; the CAS Center for Excellence in Particle Physics (CCEPP); Joint Large-Scale Scientific Facility Funds of the NSFC and CAS under Contract No. U1832207; CAS Key Research Program of Frontier Sciences under Contracts No. QYZDJ-SSW-SLH003, No. QYZDJ-SSW-SLH040; 100 Talents Program of CAS; The Institute of Nuclear and Particle Physics (INPAC) and Shanghai Key Laboratory for Particle Physics and Cosmology; European Union's Horizon 2020 research and innovation programme under Marie Sklodowska-Curie grant agreement under Contract No. 894790; German Research Foundation DFG under Contracts Nos. 455635585, Collaborative Research Center CRC 1044, FOR5327, GRK 2149; Istituto Nazionale di Fisica Nucleare, Italy; Ministry of Development of Turkey under Contract No. DPT2006K-120470; National Research Foundation of Korea under Contract No. NRF-2022R1A2C1092335; National Science and Technology fund of Mongolia; National Science Research and Innovation Fund (NSRF) via the Program Management Unit for Human Resources & Institutional Development, Research and Innovation of Thailand under Contract No. B16F640076; Polish National Science Centre under Contract No. 2019/35/O/ST2/02907; The Swedish Research Council; U.S. Department of Energy under Contract No. DE-FG02-05ER41374.

DATA AVAILABILITY

The data that support the findings of this article are openly available [1].

[1] M. Ablikim *et al.* (BESIII Collaboration), Phys. Rev. D **107**, 112001 (2023).
[2] M. Ablikim *et al.* (BESIII Collaboration), Phys. Rev. D **104**, 052006 (2021).
[3] M. Ablikim *et al.* (BESIII Collaboration), Phys. Rev. Lett. **108**, 112003 (2012).
[4] L. Zhao, N. Li, S. L. Zhu, and B. S. Zou, Phys. Rev. D **87**, 054034 (2013).
[5] Y. Dong, A. Faessler, T. Gutsche, Q. F. Lü, and V. E. Lyubovitskij, Phys. Rev. D **96**, 074027 (2017).
[6] N. Brambilla, S. Eidelman, B. K. Heltsley, R. Vogt, G. T. Bodwin, E. Eichten, A. D. Frawley, A. B. Meyer, R. E. Mitchell, V. Papadimitriou *et al.*, Eur. Phys. J. C **71**, 1534 (2011).
[7] M. Ablikim *et al.* (BESIII Collaboration), Phys. Rev. D **106**, 072004 (2022).
[8] M. Ablikim *et al.* (BESIII Collaboration), Chin. Phys. C **42**, 023001 (2018).
[9] M. Ablikim *et al.* (BESIII Collaboration), Nucl. Instrum. Methods Phys. Res., Sect. A **614**, 345 (2010).
[10] C. H. Yu *et al.*, *Proceedings of IPAC2016, Busan, Korea* (2016), 10.18429/JACoW-IPAC2016-TUYA01.
[11] M. Ablikim *et al.* (BESIII Collaboration), Chin. Phys. C **44**, 040001 (2020).
[12] J. Lu, Y. Xiao, and X. Ji, Radiat. Detect. Technol. Methods **4**, 337 (2020).
[13] J. W. Zhang *et al.*, Radiat. Detect. Technol. Methods **6**, 289 (2022).
[14] X. Li *et al.*, Radiat. Detect. Technol. Methods **1**, 13 (2017); Y. X. Guo *et al.*, Radiat. Detect. Technol. Methods **1**, 15 (2017); P. Cao *et al.*, Nucl. Instrum. Methods Phys. Res., Sect. A **953**, 163053 (2020).

[15] S. Agostinelli *et al.* (GEANT4 Collaboration), Nucl. Instrum. Methods Phys. Res., Sect. A **506**, 250 (2003).
[16] S. Jadach, B. F. L. Ward, and Z. Was, Phys. Rev. D **63**, 113009 (2001); Comput. Phys. Commun. **130**, 260 (2000).
[17] R. G. Ping, Chin. Phys. C **32**, 599 (2008); D. J. Lange, Nucl. Instrum. Methods Phys. Res., Sect. A **462**, 152 (2001).
[18] R. L. Workman *et al.* (Particle Data Group), Prog. Theor. Exp. Phys. **2022**, 083C01 (2022).
[19] J. C. Chen, G. S. Huang, X. R. Qi, D. H. Zhang, and Y. S. Zhu, Phys. Rev. D **62**, 034003 (2000); R. L. Yang, R. G. Ping, and H. Chen, Chin. Phys. Lett. **31**, 061301 (2014).
[20] D. J. Lange, Nucl. Instrum. Methods Phys. Res., Sect. A **462**, 152 (2001).
[21] Xingyu Zhou, Shuxian Du, Gang Li, and Chengping Shen, Comput. Phys. Commun. **258**, 107540 (2021).
[22] M. Ablikim *et al.* (BESIII Collaboration), Phys. Rev. D **83**, 112005 (2011).
[23] M. Ablikim *et al.* (BESIII Collaboration), Phys. Rev. D **99**, 032006 (2019).
[24] M. Ablikim *et al.* (BESIII Collaboration), Phys. Rev. D **87**, 012002 (2013).
[25] R. Wanke, How to deal with systematic uncertainties, in *Data Analysis in High Energy Physics—A Practical Guide to Statistical Methods*, edited by O. Behnke, K. Kroninger, G. Schott, and T. Schörner Sadenius (Wiley, New York, 2013), Sec. 8, ISBN 9783527410583.

M. Ablikim,[1] M. N. Achasov,[4,c] P. Adlarson,[75] O. Afedulidis,[3] X. C. Ai,[80] R. Aliberti,[35] A. Amoroso,[74a,74c] Q. An,[71,58,a] Y. Bai,[57] O. Bakina,[36] I. Balossino,[29a] Y. Ban,[46,h] H.-R. Bao,[63] V. Batozskaya,[1,44] K. Begzsuren,[32] N. Berger,[35] M. Berlowski,[44] M. Bertani,[28a] D. Bettoni,[29a] F. Bianchi,[74a,74c] E. Bianco,[74a,74c] A. Bortone,[74a,74c] I. Boyko,[36] R. A. Briere,[5] A. Brueggemann,[68] H. Cai,[76] X. Cai,[1,58] A. Calcaterra,[28a] G. F. Cao,[1,63] N. Cao,[1,63] S. A. Cetin,[62a] J. F. Chang,[1,58] G. R. Che,[43] G. Chelkov,[36,b] C. Chen,[43] C. H. Chen,[9] Chao Chen,[55] G. Chen,[1] H. S. Chen,[1,63] H. Y. Chen,[20] M. L. Chen,[1,58,63] S. J. Chen,[42] S. L. Chen,[45] S. M. Chen,[61] T. Chen,[1,63] X. R. Chen,[31,63] X. T. Chen,[1,63] Y. B. Chen,[1,58] Y. Q. Chen,[34] Z. J. Chen,[25,i] Z. Y. Chen,[1,63] S. K. Choi,[10] G. Cibinetto,[29a] F. Cossio,[74c] J. J. Cui,[50] H. L. Dai,[1,58] J. P. Dai,[78] A. Dbeyssi,[18] R. E. de Boer,[3] D. Dedovich,[36] C. Q. Deng,[72] Z. Y. Deng,[1] A. Denig,[35] I. Denysenko,[36] M. Destefanis,[74a,74c] F. De Mori,[74a,74c] B. Ding,[66,1] X. X. Ding,[46,h] Y. Ding,[34] Y. Ding,[40] J. Dong,[1,58] L. Y. Dong,[1,63] M. Y. Dong,[1,58,63] X. Dong,[76] M. C. Du,[1] S. X. Du,[80] Y. Y. Duan,[55] Z. H. Duan,[42] P. Egorov,[36,b] Y. H. Fan,[45] J. Fang,[59] J. Fang,[1,58] S. S. Fang,[1,63] W. X. Fang,[1] Y. Fang,[1] Y. Q. Fang,[1,58] R. Farinelli,[29a] L. Fava,[74b,74c] F. Feldbauer,[3] G. Felici,[28a] C. Q. Feng,[71,58] J. H. Feng,[59] Y. T. Feng,[71,58] M. Fritsch,[3] C. D. Fu,[1] J. L. Fu,[63] Y. W. Fu,[1,63] H. Gao,[63] X. B. Gao,[41] Y. N. Gao,[46,h] Yang Gao,[71,58] S. Garbolino,[74c] I. Garzia,[29a,29b] L. Ge,[80] P. T. Ge,[76] Z. W. Ge,[42] C. Geng,[59] E. M. Gersabeck,[67] A. Gilman,[69] K. Goetzen,[13] L. Gong,[40] W. X. Gong,[1,58] W. Gradl,[35] S. Gramigna,[29a,29b] M. Greco,[74a,74c] M. H. Gu,[1,58] Y. T. Gu,[15] C. Y. Guan,[1,63] A. Q. Guo,[31,63] L. B. Guo,[41] M. J. Guo,[50] R. P. Guo,[49] Y. P. Guo,[12,g] A. Guskov,[36,b] J. Gutierrez,[27] K. L. Han,[63] T. T. Han,[1] F. Hanisch,[3] X. Q. Hao,[19] F. A. Harris,[65] K. K. He,[55] K. L. He,[1,63] F. H. Heinsius,[3] C. H. Heinz,[35] Y. K. Heng,[1,58,63] C. Herold,[60] T. Holtmann,[3] P. C. Hong,[34] G. Y. Hou,[1,63] X. T. Hou,[1,63] Y. R. Hou,[63] Z. L. Hou,[1] B. Y. Hu,[59] H. M. Hu,[1,63] J. F. Hu,[56,j] S. L. Hu,[12,g] T. Hu,[1,58,63] Y. Hu,[1] G. S. Huang,[71,58] K. X. Huang,[59] L. Q. Huang,[31,63] X. T. Huang,[50] Y. P. Huang,[1] Y. S. Huang,[59] T. Hussain,[73] F. Hölzken,[3] N. Hüsken,[35] N. in der Wiesche,[68] J. Jackson,[27] S. Janchiv,[32] J. H. Jeong,[10] Q. Ji,[1] Q. P. Ji,[19] W. Ji,[1,63] X. B. Ji,[1,63] X. L. Ji,[1,58] Y. Y. Ji,[50] X. Q. Jia,[50] Z. K. Jia,[71,58] D. Jiang,[1,63] H. B. Jiang,[76] P. C. Jiang,[46,h] S. S. Jiang,[39] T. J. Jiang,[16] X. S. Jiang,[1,58,63] Y. Jiang,[63] J. B. Jiao,[50] J. K. Jiao,[34] Z. Jiao,[23] S. Jin,[42] Y. Jin,[66] M. Q. Jing,[1,63] X. M. Jing,[63] T. Johansson,[75] S. Kabana,[33] N. Kalantar-Nayestanaki,[64] X. L. Kang,[9] X. S. Kang,[40] M. Kavatsyuk,[64] B. C. Ke,[80] V. Khachatryan,[27] A. Khoukaz,[68] R. Kiuchi,[1] O. B. Kolcu,[62a] B. Kopf,[3] M. Kuessner,[3] X. Kui,[1,63] N. Kumar,[26] A. Kupsc,[44,75] W. Kühn,[37] J. J. Lane,[67] L. Lavezzi,[74a,74c] T. T. Lei,[71,58] Z. H. Lei,[71,58] M. Lellmann,[35] T. Lenz,[35] C. Li,[47] C. Li,[43] C. H. Li,[39] Cheng Li,[71,58] D. M. Li,[80] F. Li,[1,58] G. Li,[1] H. B. Li,[1,63] H. J. Li,[19] H. N. Li,[56,j] Hui Li,[43] J. R. Li,[61] J. S. Li,[59] K. Li,[1] L. J. Li,[1,63] L. K. Li,[1] Lei Li,[48] M. H. Li,[43] P. R. Li,[38,k,l] Q. M. Li,[1,63] Q. X. Li,[50] R. Li,[17,31] S. X. Li,[12] T. Li,[50] W. D. Li,[1,63] W. G. Li,[1,a] X. Li,[1,63] X. H. Li,[71,58] X. L. Li,[50] X. Y. Li,[1,63] X. Z. Li,[59] Y. G. Li,[46,h] Z. J. Li,[59] Z. Y. Li,[78] C. Liang,[42] H. Liang,[1,63] H. Liang,[71,58] Y. F. Liang,[54] Y. T. Liang,[31,63] G. R. Liao,[14] Y. P. Liao,[1,63] J. Libby,[26] A. Limphirat,[60] C. C. Lin,[55] D. X. Lin,[31,63] T. Lin,[1] B. J. Liu,[1] B. X. Liu,[76] C. Liu,[34] C. X. Liu,[1] F. Liu,[1] F. H. Liu,[53] Feng Liu,[6] G. M. Liu,[56,j] H. Liu,[38,k,l] H. B. Liu,[15] H. H. Liu,[1] H. M. Liu,[1,63] Huihui Liu,[21] J. B. Liu,[71,58] J. Y. Liu,[1,63] K. Liu,[38,k,l] K. Y. Liu,[40] Ke Liu,[22] L. Liu,[71,58] L. C. Liu,[43] Lu Liu,[43] M. H. Liu,[12,g] P. L. Liu,[1] Q. Liu,[63] S. B. Liu,[71,58] T. Liu,[12,g] W. K. Liu,[43] W. M. Liu,[71,58] X. Liu,[38,k,l] X. Liu,[39] Y. Liu,[80] Y. Liu,[38,k,l] Y. B. Liu,[43] Z. A. Liu,[1,58,63] Z. D. Liu,[9] Z. Q. Liu,[50] X. C. Lou,[1,58,63] F. X. Lu,[59] H. J. Lu,[23] J. G. Lu,[1,58] X. L. Lu,[1] Y. Lu,[7] Y. P. Lu,[1,58] Z. H. Lu,[1,63] C. L. Luo,[41] J. R. Luo,[59] M. X. Luo,[79] T. Luo,[12,g] X. L. Luo,[1,58] X. R. Lyu,[63] Y. F. Lyu,[43] F. C. Ma,[40] H. Ma,[78] H. L. Ma,[1] J. L. Ma,[1,63] L. L. Ma,[50] M. M. Ma,[1,63] Q. M. Ma,[1] R. Q. Ma,[1,63] T. Ma,[71,58] X. T. Ma,[1,63] X. Y. Ma,[1,58] Y. Ma,[46,h] Y. M. Ma,[31] F. E. Maas,[18] M. Maggiora,[74a,74c] S. Malde,[69]

Y. J. Mao,[46,h] Z. P. Mao,[1] S. Marcello,[74a,74c] Z. X. Meng,[66] J. G. Messchendorp,[13,64] G. Mezzadri,[29a] H. Miao,[1,63] T. J. Min,[42] R. E. Mitchell,[27] X. H. Mo,[1,58,63] B. Moses,[27] N. Yu. Muchnoi,[4,c] J. Muskalla,[35] Y. Nefedov,[36] F. Nerling,[18,e] L. S. Nie,[20] I. B. Nikolaev,[4,c] Z. Ning,[1,58] S. Nisar,[11,m] Q. L. Niu,[38,k,l] W. D. Niu,[55] Y. Niu,[50] S. L. Olsen,[63] Q. Ouyang,[1,58,63] S. Pacetti,[28b,28c] X. Pan,[55] Y. Pan,[57] A. Pathak,[34] Y. P. Pei,[71,58] M. Pelizaeus,[3] H. P. Peng,[71,58] Y. Y. Peng,[38,k,l] K. Peters,[13,e] J. L. Ping,[41] R. G. Ping,[1,63] S. Plura,[35] V. Prasad,[33] F. Z. Qi,[1] H. Qi,[71,58] H. R. Qi,[61] M. Qi,[42] T. Y. Qi,[12,g] S. Qian,[1,58] W. B. Qian,[63] C. F. Qiao,[63] X. K. Qiao,[80] J. J. Qin,[72] L. Q. Qin,[14] L. Y. Qin,[71,58] X. P. Qin,[12,g] X. S. Qin,[50] Z. H. Qin,[1,58] J. F. Qiu,[1] Z. H. Qu,[72] C. F. Redmer,[35] K. J. Ren,[39] A. Rivetti,[74c] M. Rolo,[74c] G. Rong,[1,63] Ch. Rosner,[18] S. N. Ruan,[43] N. Salone,[44] A. Sarantsev,[36,d] Y. Schelhaas,[35] K. Schoenning,[75] M. Scodeggio,[29a] K. Y. Shan,[12,g] W. Shan,[24] X. Y. Shan,[71,58] Z. J. Shang,[38,k,l] J. F. Shangguan,[16] L. G. Shao,[1,63] M. Shao,[71,58] C. P. Shen,[12,g] H. F. Shen,[1,8] W. H. Shen,[63] X. Y. Shen,[1,63] B. A. Shi,[63] H. Shi,[71,58] H. C. Shi,[71,58] J. L. Shi,[12,g] J. Y. Shi,[1] Q. Q. Shi,[55] S. Y. Shi,[72] X. Shi,[1,58] J. J. Song,[19] T. Z. Song,[59] W. M. Song,[34,1] Y. J. Song,[12,g] Y. X. Song,[46,h,n] S. Sosio,[74a,74c] S. Spataro,[74a,74c] F. Stieler,[35] Y. J. Su,[63] G. B. Sun,[76] G. X. Sun,[1] H. Sun,[63] H. K. Sun,[1] J. F. Sun,[19] K. Sun,[61] L. Sun,[76] S. S. Sun,[1,63] T. Sun,[51,f] W. Y. Sun,[34] Y. Sun,[9] Y. J. Sun,[71,58] Y. Z. Sun,[1] Z. Q. Sun,[1,63] Z. T. Sun,[50] C. J. Tang,[54] G. Y. Tang,[1] J. Tang,[59] M. Tang,[71,58] Y. A. Tang,[76] L. Y. Tao,[72] Q. T. Tao,[25,i] M. Tat,[69] J. X. Teng,[71,58] V. Thoren,[75] W. H. Tian,[59] Y. Tian,[31,63] Z. F. Tian,[76] I. Uman,[62b] Y. Wan,[55] S. J. Wang,[50] B. Wang,[1] B. L. Wang,[63] Bo Wang,[71,58] D. Y. Wang,[46,h] F. Wang,[72] H. J. Wang,[38,k,l] J. J. Wang,[76] J. P. Wang,[50] K. Wang,[1,58] L. L. Wang,[1] M. Wang,[50] N. Y. Wang,[63] S. Wang,[12,g] S. Wang,[38,k,l] T. Wang,[12,g] T. J. Wang,[43] W. Wang,[59] W. Wang,[72] W. P. Wang,[35,71,o] X. Wang,[46,h] X. F. Wang,[38,k,l] X. J. Wang,[39] X. L. Wang,[12,g] X. N. Wang,[1] Y. Wang,[61] Y. D. Wang,[45] Y. F. Wang,[1,58,63] Y. L. Wang,[19] Y. N. Wang,[45] Y. Q. Wang,[1] Yaqian Wang,[17] Yi Wang,[61] Z. Wang,[1,58] Z. L. Wang,[72] Z. Y. Wang,[1,63] Ziyi Wang,[63] D. H. Wei,[14] F. Weidner,[68] S. P. Wen,[1] Y. R. Wen,[39] U. Wiedner,[3] G. Wilkinson,[69] M. Wolke,[75] L. Wollenberg,[3] C. Wu,[39] J. F. Wu,[1,8] L. H. Wu,[1] L. J. Wu,[1,63] X. Wu,[12,g] X. H. Wu,[34] Y. Wu,[71,58] Y. H. Wu,[55] Y. J. Wu,[31] Z. Wu,[1,58] L. Xia,[71,58] X. M. Xian,[39] B. H. Xiang,[1,63] T. Xiang,[46,h] D. Xiao,[38,k,l] G. Y. Xiao,[42] S. Y. Xiao,[1] Y. L. Xiao,[12,g] Z. J. Xiao,[41] C. Xie,[42] X. H. Xie,[46,h] Y. Xie,[50] Y. G. Xie,[1,58] Y. H. Xie,[6] Z. P. Xie,[71,58] T. Y. Xing,[1,63] C. F. Xu,[1,63] C. J. Xu,[59] G. F. Xu,[1] H. Y. Xu,[66,2,p] M. Xu,[71,58] Q. J. Xu,[16] Q. N. Xu,[30] W. Xu,[1] W. L. Xu,[66] X. P. Xu,[55] Y. C. Xu,[77] Z. S. Xu,[63] F. Yan,[12,g] L. Yan,[12,g] W. B. Yan,[71,58] W. C. Yan,[80] X. Q. Yan,[1] H. J. Yang,[51,f] H. L. Yang,[34] H. X. Yang,[1] T. Yang,[1] Y. Yang,[12,g] Y. F. Yang,[1,63] Y. F. Yang,[43] Y. X. Yang,[1,63] Z. W. Yang,[38,k,l] Z. P. Yao,[50] M. Ye,[1,58] M. H. Ye,[8] J. H. Yin,[1] Z. Y. You,[59] B. X. Yu,[1,58,63] C. X. Yu,[43] G. Yu,[1,63] J. S. Yu,[25,i] T. Yu,[72] X. D. Yu,[46,h] Y. C. Yu,[80] C. Z. Yuan,[1,63] J. Yuan,[34] J. Yuan,[45] L. Yuan,[2] S. C. Yuan,[1,63] Y. Yuan,[1,63] Z. Y. Yuan,[59] C. X. Yue,[39] A. A. Zafar,[73] F. R. Zeng,[50] S. H. Zeng,[72] X. Zeng,[12,g] Y. Zeng,[25,i] Y. J. Zeng,[59] Y. J. Zeng,[1,63] X. Y. Zhai,[34] Y. C. Zhai,[50] Y. H. Zhan,[59] A. Q. Zhang,[1,63] B. L. Zhang,[1,63] B. X. Zhang,[1] D. H. Zhang,[43] G. Y. Zhang,[19] H. Zhang,[80] H. Zhang,[71,58] H. C. Zhang,[1,58,63] H. H. Zhang,[34] H. H. Zhang,[59] H. Q. Zhang,[1,58,63] H. R. Zhang,[71,58] H. Y. Zhang,[1,58] J. Zhang,[80] J. Zhang,[59] J. J. Zhang,[52] J. L. Zhang,[20] J. Q. Zhang,[41] J. S. Zhang,[12,g] J. W. Zhang,[1,58,63] J. X. Zhang,[38,k,l] J. Y. Zhang,[1] J. Z. Zhang,[1,63] Jianyu Zhang,[63] L. M. Zhang,[61] Lei Zhang,[42] P. Zhang,[1,63] Q. Y. Zhang,[34] R. Y. Zhang,[38,k,l] S. H. Zhang,[1,63] Shulei Zhang,[25,i] X. D. Zhang,[45] X. M. Zhang,[1] X. Y. Zhang,[50] Y. Zhang,[72] Y. Zhang,[1] Y. T. Zhang,[80] Y. H. Zhang,[1,58] Y. M. Zhang,[39] Yan Zhang,[71,58] Z. D. Zhang,[1] Z. H. Zhang,[1] Z. L. Zhang,[34] Z. Y. Zhang,[76] Z. Y. Zhang,[43] Z. Z. Zhang,[45] G. Zhao,[1] J. Y. Zhao,[1,63] J. Z. Zhao,[1,58] L. Zhao,[1] Lei Zhao,[71,58] M. G. Zhao,[43] N. Zhao,[78] R. P. Zhao,[63] S. J. Zhao,[80] Y. B. Zhao,[1,58] Y. X. Zhao,[31,63] Z. G. Zhao,[71,58] A. Zhemchugov,[36,b] B. Zheng,[72] B. M. Zheng,[34] J. P. Zheng,[1,58] W. J. Zheng,[1,63] Y. H. Zheng,[63] B. Zhong,[41] X. Zhong,[59] H. Zhou,[50] J. Y. Zhou,[34] L. P. Zhou,[1,63] S. Zhou,[6] X. Zhou,[76] X. K. Zhou,[6] X. R. Zhou,[71,58] X. Y. Zhou,[39] Y. Z. Zhou,[12,g] J. Zhu,[43] K. Zhu,[1] K. J. Zhu,[1,58,63] K. S. Zhu,[12,g] L. Zhu,[34] L. X. Zhu,[63] S. H. Zhu,[70] T. J. Zhu,[12,g] W. D. Zhu,[41] Y. C. Zhu,[71,58] Z. A. Zhu,[1,63] J. H. Zou,[1] and J. Zu[71,58]

(BESIII Collaboration)

[1]*Institute of High Energy Physics, Beijing 100049, People's Republic of China*
[2]*Beihang University, Beijing 100191, People's Republic of China*
[3]*Bochum Ruhr-University, D-44780 Bochum, Germany*
[4]*Budker Institute of Nuclear Physics SB RAS (BINP), Novosibirsk 630090, Russia*
[5]*Carnegie Mellon University, Pittsburgh, Pennsylvania 15213, USA*
[6]*Central China Normal University, Wuhan 430079, People's Republic of China*
[7]*Central South University, Changsha 410083, People's Republic of China*
[8]*China Center of Advanced Science and Technology, Beijing 100190, People's Republic of China*
[9]*China University of Geosciences, Wuhan 430074, People's Republic of China*

[10]*Chung-Ang University, Seoul, 06974, Republic of Korea*
[11]*COMSATS University Islamabad, Lahore Campus, Defence Road, Off Raiwind Road, 54000 Lahore, Pakistan*
[12]*Fudan University, Shanghai 200433, People's Republic of China*
[13]*GSI Helmholtzcentre for Heavy Ion Research GmbH, D-64291 Darmstadt, Germany*
[14]*Guangxi Normal University, Guilin 541004, People's Republic of China*
[15]*Guangxi University, Nanning 530004, People's Republic of China*
[16]*Hangzhou Normal University, Hangzhou 310036, People's Republic of China*
[17]*Hebei University, Baoding 071002, People's Republic of China*
[18]*Helmholtz Institute Mainz, Staudinger Weg 18, D-55099 Mainz, Germany*
[19]*Henan Normal University, Xinxiang 453007, People's Republic of China*
[20]*Henan University, Kaifeng 475004, People's Republic of China*
[21]*Henan University of Science and Technology, Luoyang 471003, People's Republic of China*
[22]*Henan University of Technology, Zhengzhou 450001, People's Republic of China*
[23]*Huangshan College, Huangshan 245000, People's Republic of China*
[24]*Hunan Normal University, Changsha 410081, People's Republic of China*
[25]*Hunan University, Changsha 410082, People's Republic of China*
[26]*Indian Institute of Technology Madras, Chennai 600036, India*
[27]*Indiana University, Bloomington, Indiana 47405, USA*
[28a]*INFN Laboratori Nazionali di Frascati, I-00044, Frascati, Italy*
[28b]*INFN Sezione di Perugia, I-06100, Perugia, Italy*
[28c]*University of Perugia, I-06100, Perugia, Italy*
[29a]*INFN Sezione di Ferrara, I-44122, Ferrara, Italy*
[29b]*University of Ferrara, I-44122, Ferrara, Italy*
[30]*Inner Mongolia University, Hohhot 010021, People's Republic of China*
[31]*Institute of Modern Physics, Lanzhou 730000, People's Republic of China*
[32]*Institute of Physics and Technology, Peace Avenue 54B, Ulaanbaatar 13330, Mongolia*
[33]*Instituto de Alta Investigación, Universidad de Tarapacá, Casilla 7D, Arica 1000000, Chile*
[34]*Jilin University, Changchun 130012, People's Republic of China*
[35]*Johannes Gutenberg University of Mainz, Johann-Joachim-Becher-Weg 45, D-55099 Mainz, Germany*
[36]*Joint Institute for Nuclear Research, 141980 Dubna, Moscow region, Russia*
[37]*Justus-Liebig-Universitaet Giessen, II. Physikalisches Institut, Heinrich-Buff-Ring 16, D-35392 Giessen, Germany*
[38]*Lanzhou University, Lanzhou 730000, People's Republic of China*
[39]*Liaoning Normal University, Dalian 116029, People's Republic of China*
[40]*Liaoning University, Shenyang 110036, People's Republic of China*
[41]*Nanjing Normal University, Nanjing 210023, People's Republic of China*
[42]*Nanjing University, Nanjing 210093, People's Republic of China*
[43]*Nankai University, Tianjin 300071, People's Republic of China*
[44]*National Centre for Nuclear Research, Warsaw 02-093, Poland*
[45]*North China Electric Power University, Beijing 102206, People's Republic of China*
[46]*Peking University, Beijing 100871, People's Republic of China*
[47]*Qufu Normal University, Qufu 273165, People's Republic of China*
[48]*Renmin University of China, Beijing 100872, People's Republic of China*
[49]*Shandong Normal University, Jinan 250014, People's Republic of China*
[50]*Shandong University, Jinan 250100, People's Republic of China*
[51]*Shanghai Jiao Tong University, Shanghai 200240, People's Republic of China*
[52]*Shanxi Normal University, Linfen 041004, People's Republic of China*
[53]*Shanxi University, Taiyuan 030006, People's Republic of China*
[54]*Sichuan University, Chengdu 610064, People's Republic of China*
[55]*Soochow University, Suzhou 215006, People's Republic of China*
[56]*South China Normal University, Guangzhou 510006, People's Republic of China*
[57]*Southeast University, Nanjing 211100, People's Republic of China*
[58]*State Key Laboratory of Particle Detection and Electronics, Beijing 100049, Hefei 230026, People's Republic of China*
[59]*Sun Yat-Sen University, Guangzhou 510275, People's Republic of China*
[60]*Suranaree University of Technology, University Avenue 111, Nakhon Ratchasima 30000, Thailand*
[61]*Tsinghua University, Beijing 100084, People's Republic of China*
[62a]*Turkish Accelerator Center Particle Factory Group, Istinye University, 34010, Istanbul, Turkey*
[62b]*Near East University, Nicosia, North Cyprus, 99138, Mersin 10, Turkey*

[63]University of Chinese Academy of Sciences, Beijing 100049, People's Republic of China
[64]University of Groningen, NL-9747 AA Groningen, The Netherlands
[65]University of Hawaii, Honolulu, Hawaii 96822, USA
[66]University of Jinan, Jinan 250022, People's Republic of China
[67]University of Manchester, Oxford Road, Manchester, M13 9PL, United Kingdom
[68]University of Muenster, Wilhelm-Klemm-Strasse 9, 48149 Muenster, Germany
[69]University of Oxford, Keble Road, Oxford OX13RH, United Kingdom
[70]University of Science and Technology Liaoning, Anshan 114051, People's Republic of China
[71]University of Science and Technology of China, Hefei 230026, People's Republic of China
[72]University of South China, Hengyang 421001, People's Republic of China
[73]University of the Punjab, Lahore-54590, Pakistan
[74a]University of Turin, I-10125, Turin, Italy
[74b]University of Eastern Piedmont, I-15121, Alessandria, Italy
[74c]INFN, I-10125, Turin, Italy
[75]Uppsala University, Box 516, SE-75120 Uppsala, Sweden
[76]Wuhan University, Wuhan 430072, People's Republic of China
[77]Yantai University, Yantai 264005, People's Republic of China
[78]Yunnan University, Kunming 650500, People's Republic of China
[79]Zhejiang University, Hangzhou 310027, People's Republic of China
[80]Zhengzhou University, Zhengzhou 450001, People's Republic of China

[a]Deceased.
[b]Also at the Moscow Institute of Physics and Technology, Moscow 141700, Russia.
[c]Also at the Novosibirsk State University, Novosibirsk, 630090, Russia.
[d]Also at the NRC "Kurchatov Institute," PNPI, 188300, Gatchina, Russia.
[e]Also at Goethe University Frankfurt, 60323 Frankfurt am Main, Germany.
[f]Also at Key Laboratory for Particle Physics, Astrophysics and Cosmology, Ministry of Education; Shanghai Key Laboratory for Particle Physics and Cosmology; Institute of Nuclear and Particle Physics, Shanghai 200240, People's Republic of China.
[g]Also at Key Laboratory of Nuclear Physics and Ion-beam Application (MOE) and Institute of Modern Physics, Fudan University, Shanghai 200443, People's Republic of China.
[h]Also at State Key Laboratory of Nuclear Physics and Technology, Peking University, Beijing 100871, People's Republic of China.
[i]Also at School of Physics and Electronics, Hunan University, Changsha 410082, China.
[j]Also at Guangdong Provincial Key Laboratory of Nuclear Science, Institute of Quantum Matter, South China Normal University, Guangzhou 510006, China.
[k]Also at MOE Frontiers Science Center for Rare Isotopes, Lanzhou University, Lanzhou 730000, People's Republic of China.
[l]Also at Lanzhou Center for Theoretical Physics, Lanzhou University, Lanzhou 730000, People's Republic of China.
[m]Also at the Department of Mathematical Sciences, IBA, Karachi 75270, Pakistan.
[n]Also at Ecole Polytechnique Federale de Lausanne (EPFL), CH-1015 Lausanne, Switzerland.
[o]Also at Helmholtz Institute Mainz, Staudinger Weg 18, D-55099 Mainz, Germany.
[p]Also at School of Physics, Beihang University, Beijing 100191, China.